treatment of iHO with rhIL-22 and microinjection with SL1344. These findings were demonstrated via RT-qPCR and immunostaining (**Figure 4.14**).

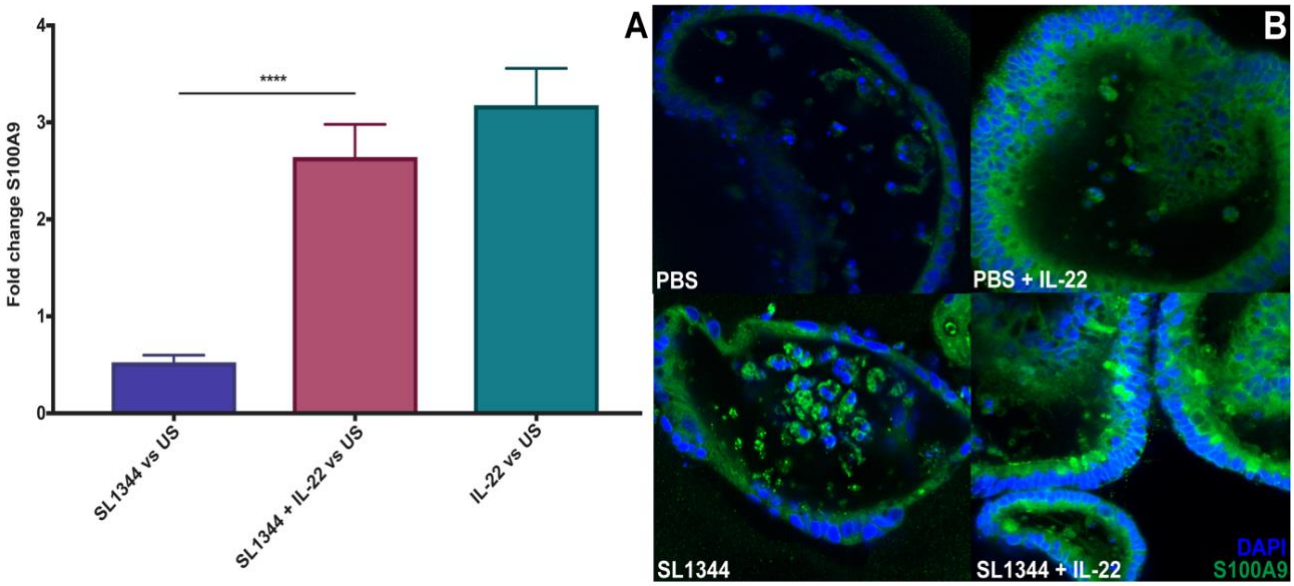

Figure 4.14: Increased expression of S100A9 in iHO pre-treated with rhIL-22. (**A**) iHO were either left unstimulated, or treated for 18 hours with rhIL-22 at 100 ng/mL. iHO were then left uninfected or injected with SL1344 and incubated for 3 hours, followed by harvesting and RNA extraction. RT-qPCR with TaqMan gene expression assay for S100A9 was then completed to compare S100A9 expression between treatment groups and unstimulated iHO. Data presented are fold change in expression of S100A9, averaged from 4 technical replicates, with assays repeated 3 times. Data were analysed using the comparative cycle threshold (C_T) method, with GAPDH as an endogenous control. Unpaired student's t-test was used to compare results (****$p < 0.0001$). A significant difference in S100A9 expression was noted in SL1344-infected iHO pre-treated with rhIL-22 versus those left untreated. (**B**) Kolf2 iHO pre-treated with rhIL-22 for 18 hours at 100 ng/mL, or left unstimulated, were microinjected with PBS (control) or SL1344 and incubated for 3 hours, before fixing and immunostaining for nuclei with DAPI (blue) and S100A9 expression (green). Increased intensity of S100A9 staining was demonstrated in samples treated with rhIL-22 and exposed to bacteria, with maximal staining seen in iHO both pre-treated with rhIL-22 and infected. Images taken on Zeiss LSM 510 Meta confocal microscope at 20x magnification.

IL-22 has been shown to upregulate S100A9 production in fibroblast-like synoviocytes, via induction of STAT3 phosphorylation,[25] therefore, given the findings on qPCR / immunostaining, the role of S100A9 in phagolysosomal fusion was further investigated by the use of hiPSC with a biallelic mutation in the S100A9 gene ($S100A9^{-/-}$). This cell line was produced by the Cellular Generation and Phenotyping (CGaP) facility at the Wellcome Trust Sanger Institute, via CRISPR/Cas9 engineering, as outlined in 2.10/Appendix 2. Organoids were differentiated from hiPSC as previously described and phenotyped via immunostaining and RT-qPCR, with no morphological differences noted between iHO generated from $S100A9^{-/-}$ and Kolf2 cell lines (**Figure 4.15**).

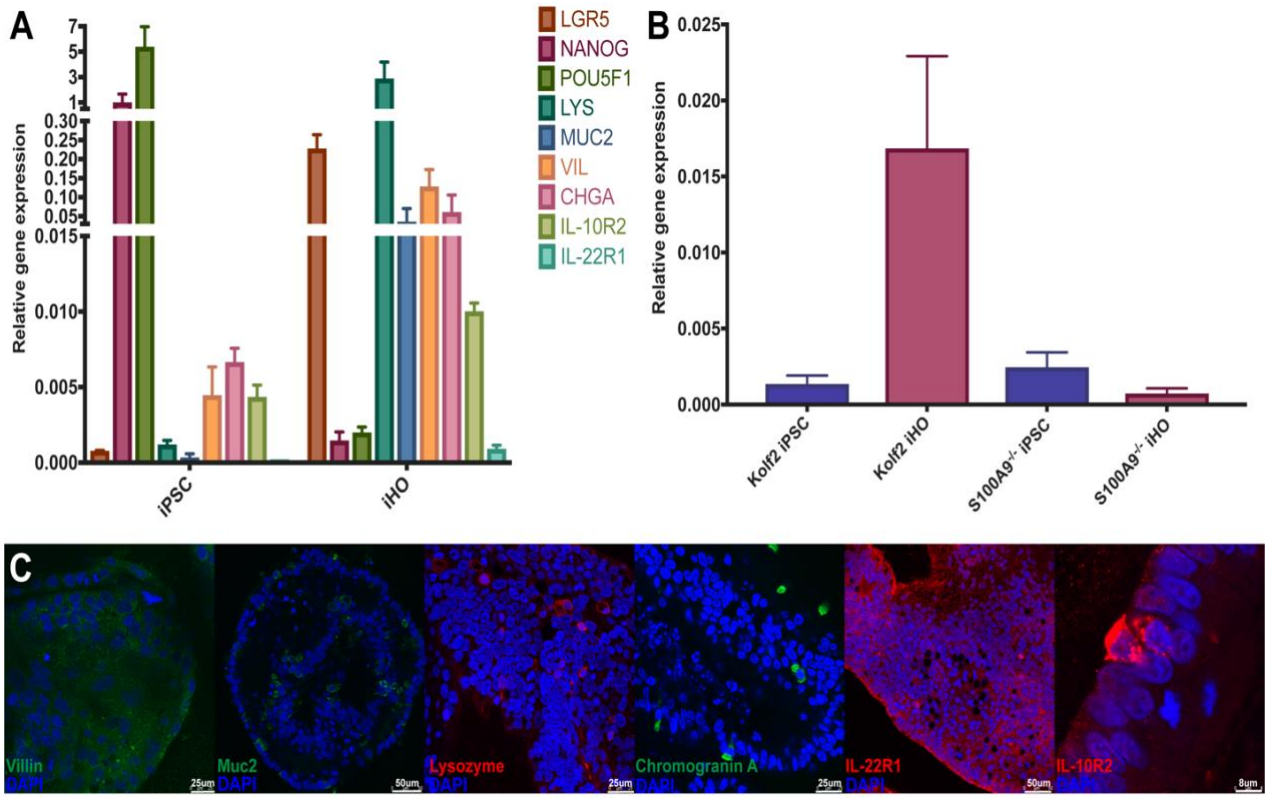

Figure 4.15: Phenotyping of iHO generated from S100A9$^{-/-}$ cell line. (**A**) Relative expression of genes in S100A9$^{-/-}$ iPSC versus iHO, demonstrating that markers of pluripotency (NANOG, POU5F) are highly expressed in iPSC, whereas genes coding for specific cell types (Vil1, Lys, Muc2, ChgA) and stem cells (LGR5) are highly expressed in iHO, denoting differentiation. Data presented are from 4 technical replicates, with assays repeated 3 times using paired iPSC/iHO of different batches. Data were analysed using the comparative cycle threshold (C_T) method, with GAPDH as an endogenous control. (**B**) Expression of S100A9 in Kolf2 iPSC/iHO versus S100A9$^{-/-}$ iPSC/iHO, demonstrating expression of S100A9 in Kolf2 iHO, but minimal expression in S100A9$^{-/-}$ iHO. (**C**) Immunostaining of S100A9$^{-/-}$ iHO to demonstrate presence of constituent intestinal cell types. Imaged are iHO with nuclei stained with DAPI (blue) and for the presence of: Villin, Mucin2, Chromogranin A (green), Lysozyme, IL-22R1 and IL10R2 (red). Images taken on the Leica SP8 confocal microscope at 20x (Villin, Muc2, Lysozyme, Chromogranin A, IL-22R1) or 40x (IL-10R2) magnification.

No expression of S100A9 protein or Rab7 expression was detected using immunostaining following IL-22 stimulation and infection with SL1344 in S100A9$^{-/-}$ iHO (**Figure 4.16 A&B**). iHO from both cell lines were stimulated with rhIL-22 and dissociated, then stained with S100A9 antibody and FACS sorted. Increased S100A9 expression was seen in Kolf2 iHO versus S100A9$^{-/-}$ iHO (**Figure 4.16 C**). Gentamicin protection assays in S100A9$^{-/-}$ iHO demonstrated no significant difference in intracellular bacterial counts of SL1344 in rhIL-22 treated versus untreated S100A9$^{-/-}$ iHO (**Figure 4.16 D**). These data suggest that S100A9, induced by IL-22, inhibits SL1344 infection in the intestinal epithelium.

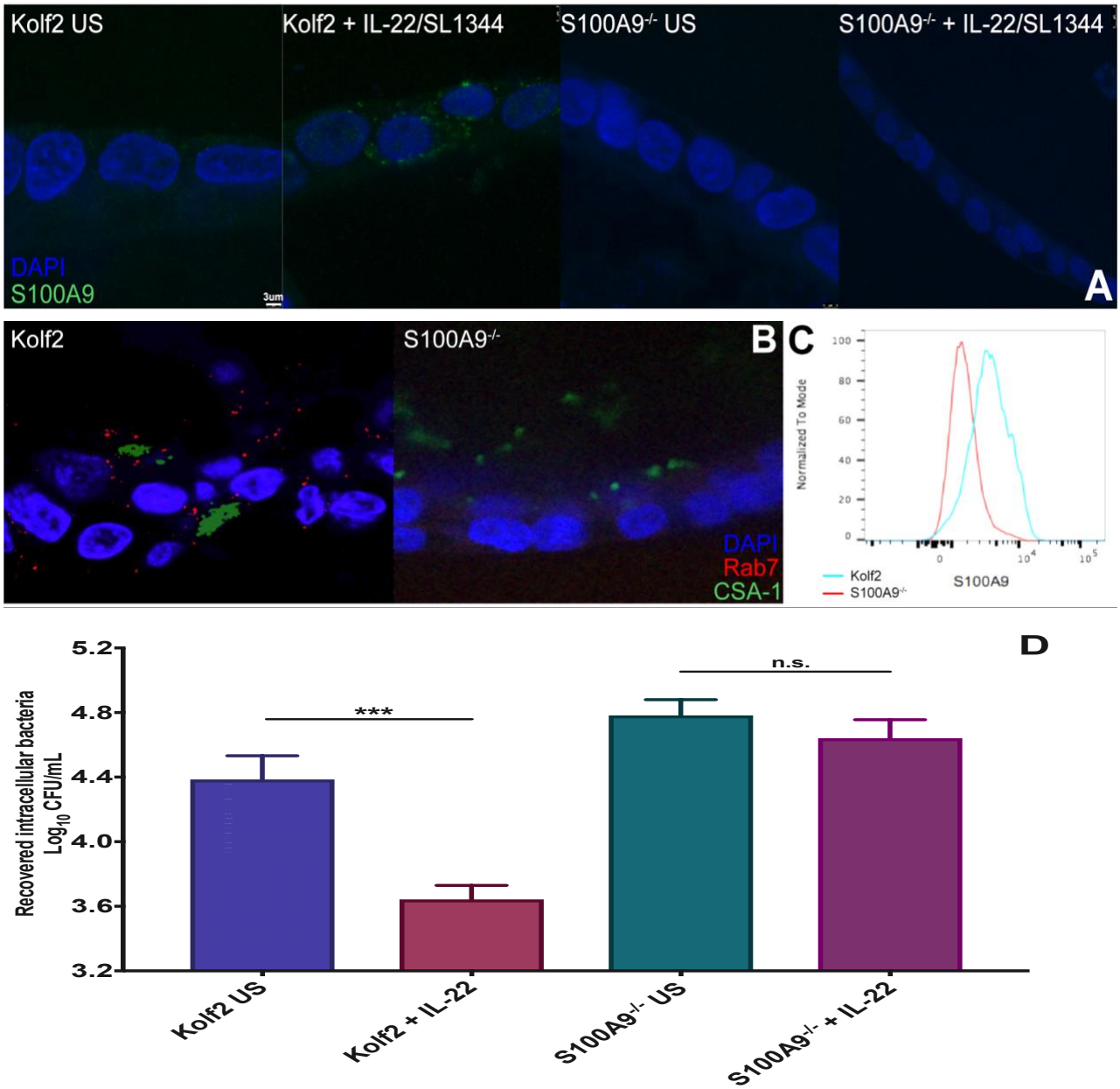

Figure 4.16: IL-22 induces S100A9-mediated protection from SL1344 infection. (**A**) Kolf2 and S100A9$^{-/-}$ iHO were pre-treated with rhIL-22 for 18 hours at 100 ng/mL or left unstimulated, then injected with SL1344, followed by incubation for 3 hours, fixing and immunostaining. (**A**) S100A9 protein (green) expression is demonstrated in Kolf2, but not S100A9$^{-/-}$ iHO. (**B**) Kolf2 and S100A9$^{-/-}$ iHO were pre-treated with rhIL-22 at 100 ng/mL for 18 hours and injected with SL1344, followed by fixing and immunostaining for DAPI (blue), CSA-1 (green) and RAB7 (red). RAB7 was expressed in Kolf2 iHO but not in S100A9$^{-/-}$ iHO. Images for **A** & **B** were taken on the Leica SP8 confocal microscope at 40x magnification. (**C**) Kolf2 and S100A9$^{-/-}$ iHO were pre-stimulated with rhIL-22 at 100 ng/mL for 18 hours, dissociated into single cells, stained and FACS sorted. Histogram showing expression of S100A9 demonstrates increased S100A9 expression in Kolf2 iHO. (**D**) Kolf2 and S100A9$^{-/-}$ iHO were pre-treated with rhIL-22 for 18 hours at 100 ng/mL or left unstimulated, then injected with SL1344 and incubated for 1.5 hours, before undergoing modified gentamicin protection assays for recovery of intracellular bacteria. Data presented are for 3 biological replicates (each averaged from 3 technical replicates), with 30 iHO injected per replicate +/- SEM. Unpaired Mann-Whitney tests were used to compare results (**n.s.** not significant, *** p<0.001). Significantly fewer bacteria were recovered intracellularly in Kolf2 iHO pre-treated with rhIL-22 before SL1344 infection. No significant difference is seen between treated and untreated S100A9$^{-/-}$ iHO.

To confirm that S100A9$^{-/-}$ iHO were able to produce a response to IL-22 in aspects other than S100A9 secretion, iHO were stimulated with rhIL-22 for 18 hours and RT-qPCR completed to measure expression of IL-22 regulated genes DUOX2 and LCN2. There was a significant increase in expression of both genes following IL-22 treatment (**Figure 4.17**).

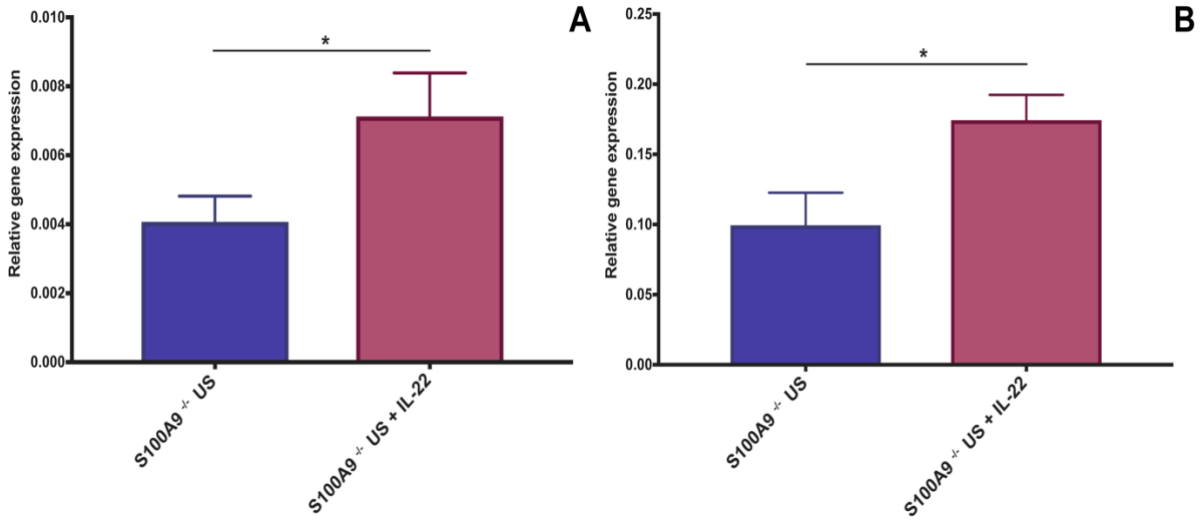

Figure 4.17: Relative gene expression of IL-22 regulated genes DUOX2 and LCN2 in S100A9$^{-/-}$ iHO. S100A9$^{-/-}$ iHO were treated with rhIL-22 at 100 ng/mL for 18 hours or left unstimulated. RNA was harvested and RT-qPCR completed to compare expression of IL-22 regulated genes DUOX2 (Panel **A**) and LCN2 (Panel **B**). Data presented are from 4 technical replicates, with assays repeated 3 times. Data were analysed using the comparative cycle threshold (C_T) method, with GAPDH as an endogenous control. Unpaired Mann-Whitney test was used to compare results (*$p < 0.05$). Expression of DUOX2 (**A**) and LCN2 (**B**) is significantly upregulated in response to rhIL-22 treatment in S100A9$^{-/-}$ iHO, demonstrating that S100A9$^{-/-}$ iHO retain the ability to respond to IL-22.

4.8 Single cell responses after IL-22 stimulation

Although the mechanism for the restrictive effect of IL-22 on *S*. Typhimurium SL1344 by phagolysosomal fusion has been demonstrated via a number of methods, the specific cell types responding to IL-22 and the transcriptional changes that occur within these cells have yet to be elucidated. A small-scale trial of single cell sequencing of unstimulated Kolf2 iHO and those pre-treated with rhIL-22 was completed to begin to address this. Methods for cell sorting, barcoding, sequencing and data analysis are described in 2.7/Appendix 1. For the remaining figures in this chapter, 'Unstimulated' refers to single cells from iHO not pre-treated and 'IL-22 stimulated' refers to single cells from iHO treated for 18 hours at 100 ng/mL. As an initial method of quality control and responsiveness to IL-22 in the cells sequenced, remaining RNA following sample submission for RNA-Seq was transcribed and RT-qPCR completed. Both LCN2 and IFITM3 were significantly upregulated in rhIL-22 treated

cells, but interestingly there was a large degree of variation between cells in terms of levels of relative gene expression (**Figure 4.18**).

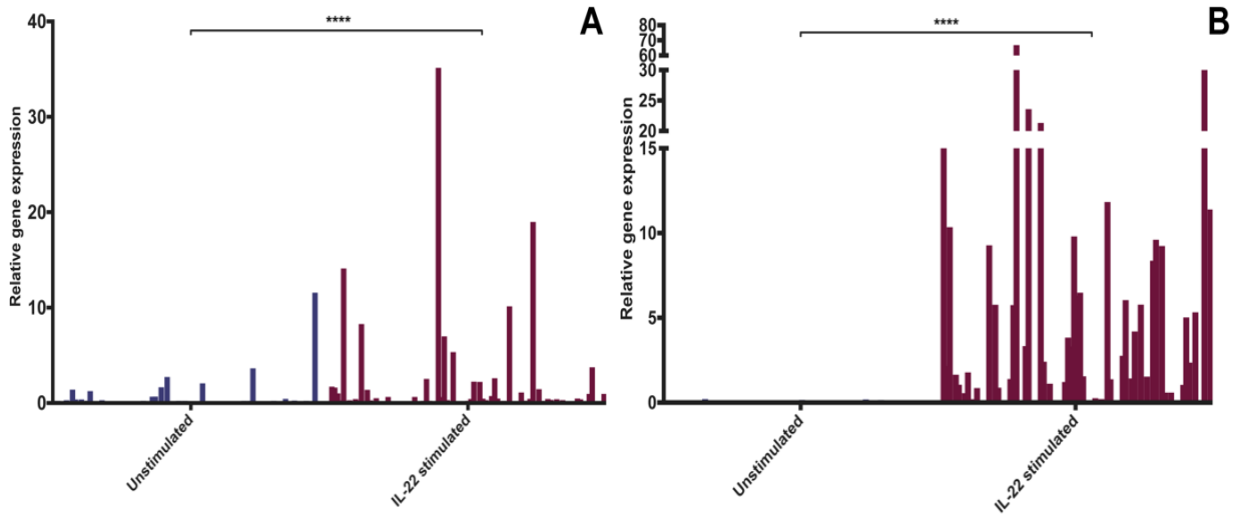

Figure 4.18: Relative gene expression of IL-22 regulated genes LCN2 and IFITM3 in rhIL-22 stimulated and unstimulated single cells. RT-qPCR was completed to compare expression of LCN2 and IFITM3 between single cells from IL-22 stimulated and unstimulated iHO. Data presented are from 1 technical replicate, with assays repeated once. Each bar represents a single cell. Data were analysed using the comparative cycle threshold (C_T) method, with GAPDH as an endogenous control. Unpaired Mann-Whitney test was used to compare results (****$p < 0.0001$). (**A**) LCN2 and (**B**) IFITM3 are significantly upregulated in response to rhIL-22 treatment.

The Single Cell Consensus Clustering (SC3) programme[26] and Seurat package[27] were used to examine the data, and G:Profiler (https://biit.cs.ut.ee/gprofiler/gost) to look at differential enrichment data. SC3 is an unsupervised clustering approach which uses parallelisation to simultaneously analyse multiple clustering solutions, which are then combined into a consensus matrix summarising how frequently each pair of cells is placed in the same cluster and thus similarity between cells. The results of the consensus matrix then undergo complete-linkage hierarchical clustering into *k* groups. The program is also able to identify differentially expressed genes, which are genes that vary between two or more clusters, and identify marker genes, which are genes highly expressed in one particular cell cluster and able to distinguish this cluster from the remaining ones. In order to identify marker genes, a binary classifier for each gene is produced from mean cluster-expression values, and the area under ROC curve is used to quantify how accurate these predictions are. Each gene receives a p-value using the Wilcoxon signed-rank test, which allows comparison of gene ranks in the cluster with the highest mean expression with all others. Marker genes are defined as those with an area under the ROC curve of >0.85 and $p<0.01$.

Firstly, PCA plots were used to look at clustering by IL-22 status (cohort). Interestingly, there did not appear to be a distinct separation between cells based on cohort, which demonstrates a lack of plate effect, but also that an alternative factor was the primary driver of differences between cell groups. This was confirmed on clustering analysis, which suggested 4 primary clusters of cells, but that cells from each cohort were to be found in each cluster (**Figure 4.19**).

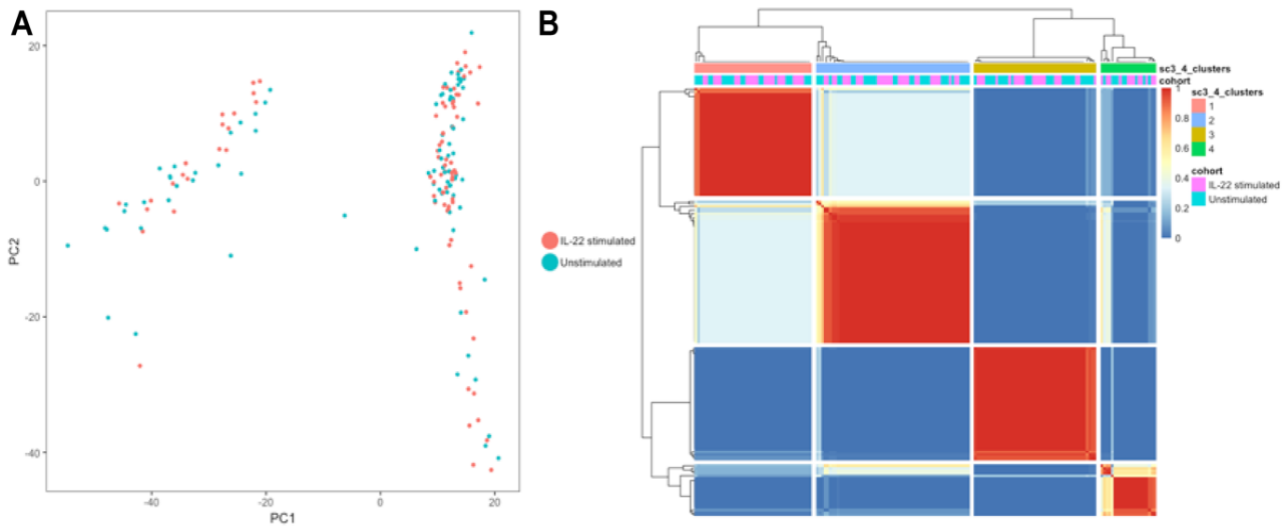

Figure 4.19: PCA and clustering analysis for all cells using SC3. (**A**) PCA of all cells by cohort, with mixing of IL-22 stimulated and unstimulated cells. (**B**) Clustering analysis; similarity of 1 (red) indicates that the two cells are always assigned to the same cluster and suggests robustness of clustering strategy. Four clusters were suggested by the analysis, each containing a mix of unstimulated and IL-22 stimulated cells. Images generated using SC3 package.

Using Seurat to interrogate PCAs, (following scaling for UMIs and mitochondrial gene content) suggested that for all cells, PC1 was primarily defined by MAP1B – microtubule related protein important for maintaining cell structure; other elements of this PC included genes related to epithelial cell differentiation and cell-cell adhesion. PC2 was defined by a number of cell cycle related genes, including CKS1B, MAD2L1, HMGN2, HMGB2, CKS2, MKI67 and TOP2A (**Figure 4.20**). PCAs were also run for cells by cohort, with PC1 for the unstimulated group being made up of genes responsible for cell-cell adhesion, and protein localisation to the plasma membrane and PC2 cell development and differentiation. For IL-22 stimulated cells, PC1 was dominated by genes responsible for extracellular and phagocytic vesicle membrane production and PC2 regulation of cytokine production, platelet derived growth factor signalling and negative regulation of cell differentiation. The

upregulation of these genes in the IL-22 stimulated group makes biological sense, given the mechanism established in this thesis for the role of IL-22 in increased phagolysosomal fusion, and in response to infection / inflammation wherein it is known to increase cell proliferation, decrease differentiation and induce a secretory response for defence of the epithelium.[2,28]

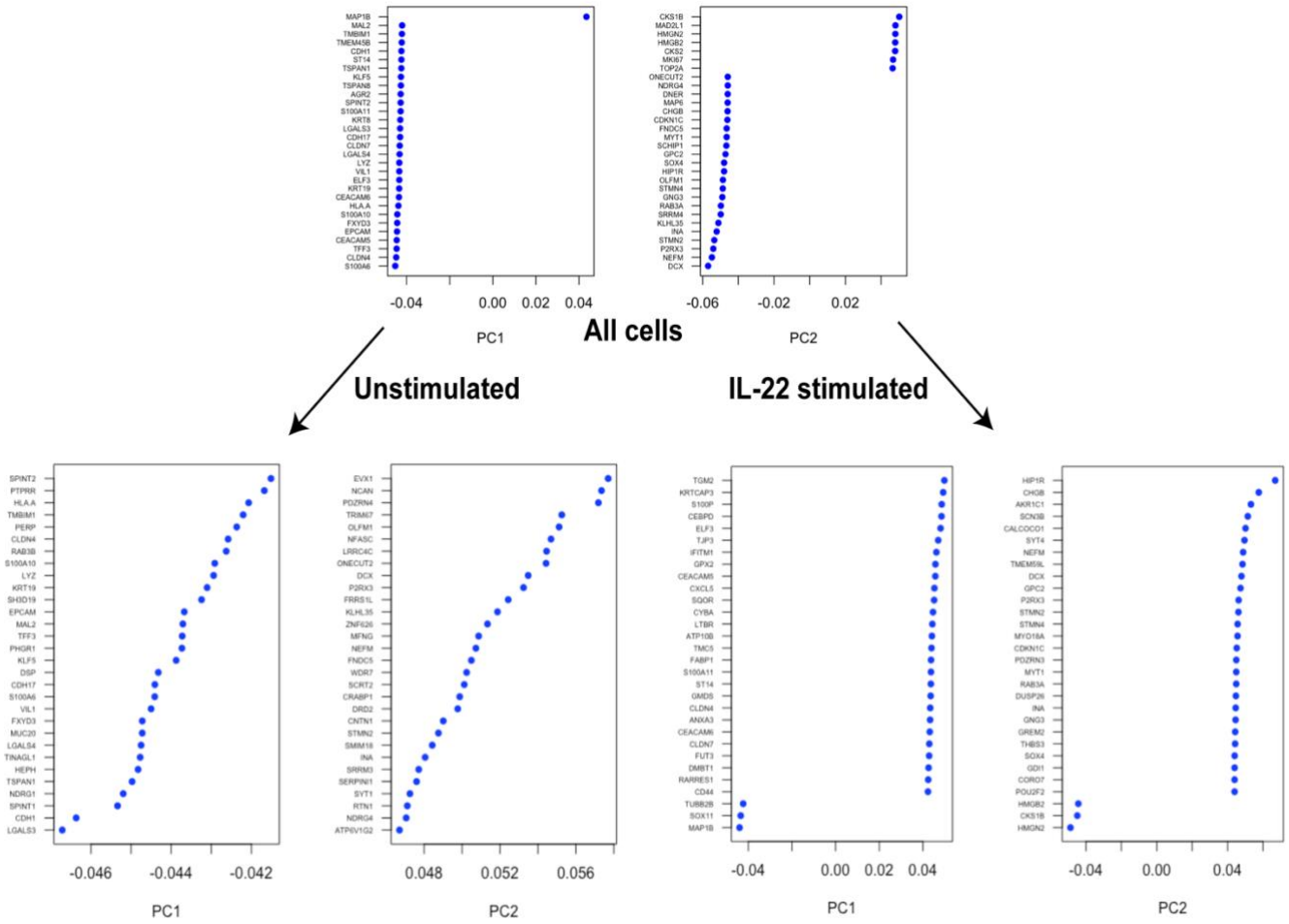

Figure 4.20: PCA for all cells and subsets using Seurat. PC1 and PC2 for all cells, with subdivision into PCs for unstimulated and IL-22 stimulated cells. Plotted are the top 30 genes influencing PC for each group. Images generated using Seurat package.

Differential expression (DE) and clustering analysis was performed using SC3. DE was calculated using the Kruskal-Wallis test. A significant p value demonstrates that gene expression in at least 1 cluster dominates 1 other cluster. For unstimulated cells, SC3 denoted 4 clusters, identifying 880 differentially expressed genes based on this clustering. The top 10 marker genes for each cluster are represented in the plots in **Figure 4.21**. Cluster 1 contains genes responsible for cell-cell adhesion and production of extracellular organelles, cluster 2 - cell cycle, cluster 3 – cell signalling / amino acid transport and cluster

4 - neurogenesis. For IL-22 stimulated cells, SC3 denoted 5 clusters, with 894 differentially expressed genes based on this clustering. Marker genes for clusters suggested the following functions: cluster 1 - extracellular exosome and vesicle production / prostaglandin synthesis, cluster 2 - cell cycle, cluster 3 – (Vimentin); a cytoskeletal protein involved in cell migration and signalling (bacterial and viral pathogen attachment), cluster 4 - cell-cell signalling and neurogenesis, cluster 5 - (C8orf46) neurogenesis.

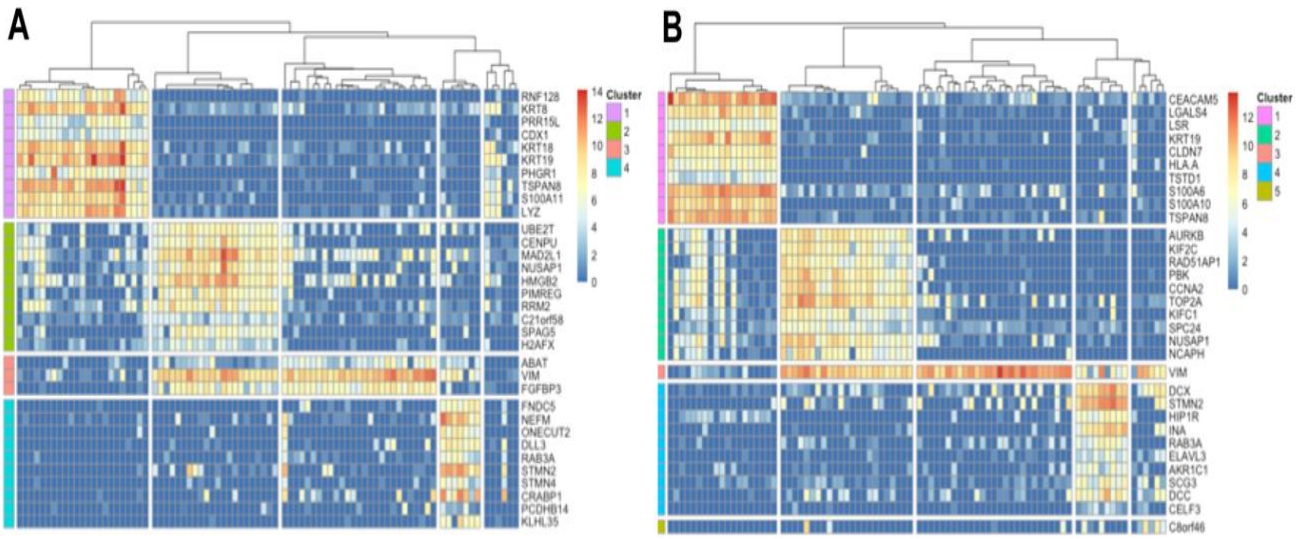

Figure 4.21: Differential expression and marker gene analysis for cohorts using SC3. Differential expression matrix (cells in columns, genes in rows) for unstimulated (**A**) and IL-22 stimulated (**B**) cells, delineating the cell clusters, and listing up to the top 10 marker genes for each cluster. Images generated using SC3 package.

In comparison to the clustering done using SC3, T-SNE plotting using Seurat suggested 3 clusters when using all cohorts. These clusters were interrogated by using known cell type markers to assess whether it was possible to discern whether particular cell types (e.g. secretory cells) clustered together. Markers for cell types searched included: enterocytes, goblet cells, stem cells, enteroendocrine cells, Paneth cells and cell cycle related genes. Plots for each cohort separately did not differ to those produced for all cells, therefore plots for all cells are represented below (**Figure 4.22**). Importantly, IL-10R2 appeared to be expressed by multiple cell clusters, suggesting that whilst it may be expressed strongly on enteroendocrine cells (as noted on immunostaining in **Figure 4.3**), it also appears to be expressed on other IEC types.

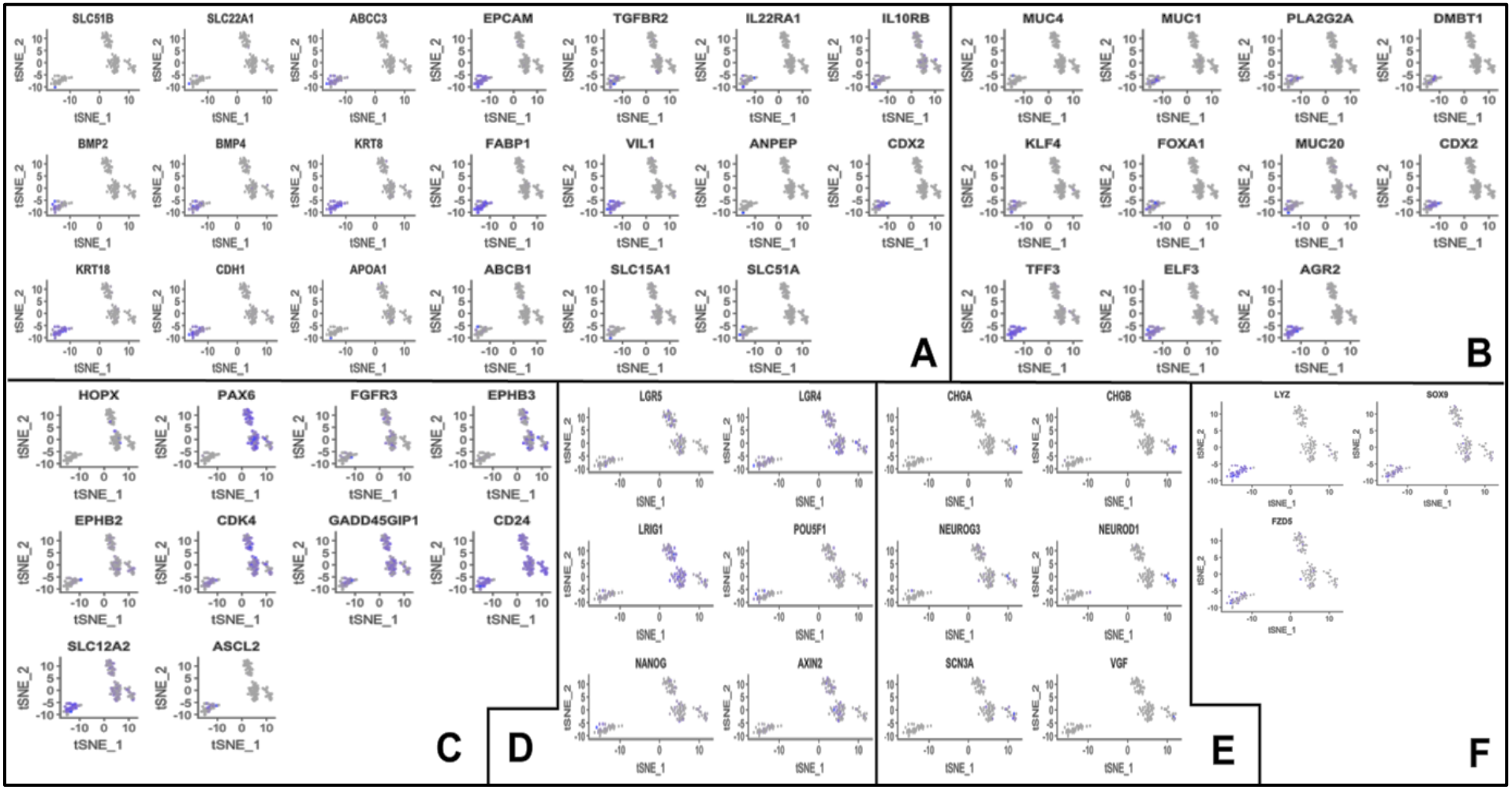

Figure 4.22 – Investigating cell types using known gene markers. Data are t-SNE plots representing all cells, with cells positive for the listed gene highlighted in purple. Data represent cells from iHO both unstimulated and IL-22 stimulated. (**A**) are genes expected on enterocytes, (**B**) goblet cells, (**C**) cell cycle genes, (**D**) stem cells, (**E**) enteroendocrine cells and (**F**) Paneth cells. Plots constructed using Seurat package.

Based on t-SNE clustering (**Figure 4.23**) and interrogation of gene markers, there is a clearly delineated cluster of cells (cluster 1) which look to be differentiated enterocytes / secretory cells, whereas clusters 0 and 2 are marked by cell cycle and stem cell related genes. This fits with clustering run by this programme, which denoted a combination of cytoskeletal and cell cycle genes in cluster 0, extracellular vesicle/organelle related genes in cluster 1 and cell cycle genes in cluster 2. Interestingly, (as seen in **Figure 4.22**) enteroendocrine cells appeared to cluster in the outer part of cluster 0, rather than with the other secretory cells.

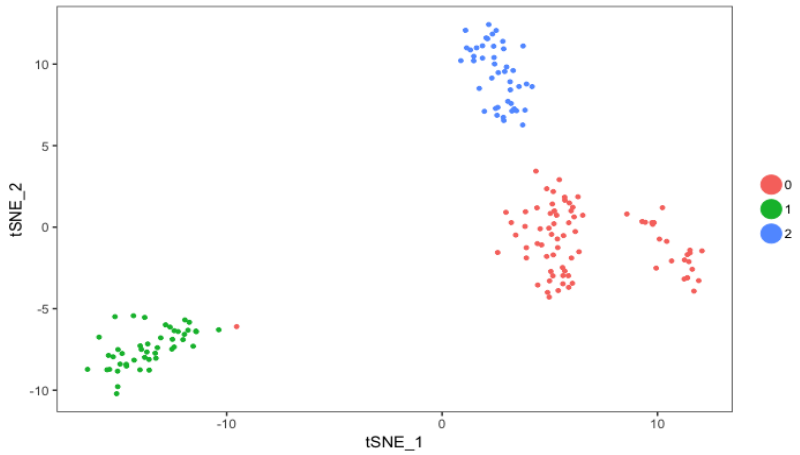

Figure 4.23 – t-SNE plot for all cells using Seurat. This plot includes both unstimulated and IL-22 stimulated cells. Cells are divided into 3 clusters. Based on interrogation with gene markers, cluster 1 are likely enterocytes / secretory cells, clusters 0 and 2 contain high proportions of cell cycling / stem cell gene markers.

Plots were made of the top 30 IL-22 upregulated genes in all cells, and demonstrated that these genes were located within all cell clusters, reinforcing what was seen on imaging about the ubiquity of the IL-22 receptor on all cell types (**Figure 4.24**). The genes upregulated were those expected as part of the epithelial defensive response to pathogens, (IFITM1, IFITM2, IFITM3, LCN2, DUOX2, DMBT1, MUC1 and MUC4), those which are a part of the phagolysosomal fusion pathway (RAB7A, LAMP1, S100A9), the JAK/STAT pathway (JAK1, STAT3, IL-23A) and those responsible for antimicrobial peptide production (PLA2G2A) and the innate immune response (TIFA, CEACAM1, SERPINA3). Given the limited number of cells in the cohort and the dominance of cell cycle genes in most cells sequenced, it is difficult to draw further conclusions about the effect of IL-22 on single cells.

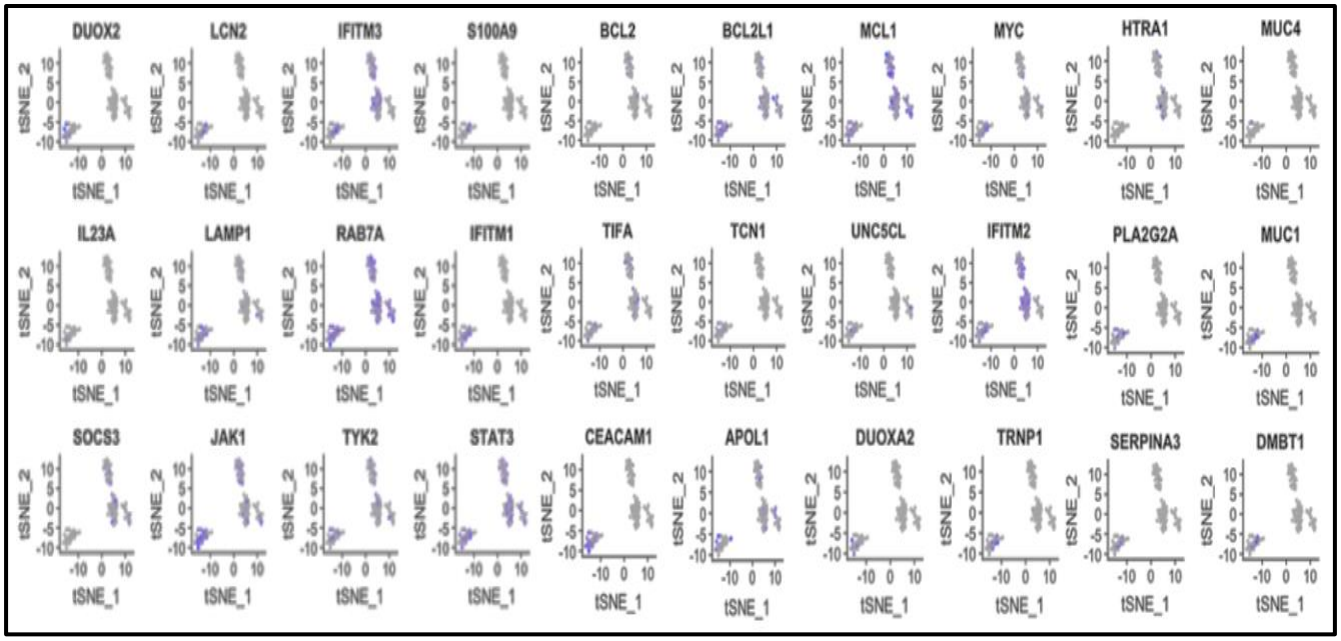

Figure 4.24 – Top 30 IL-22 upregulated genes. Plots represent all cells (both unstimulated and IL-22 stimulated), with cells expressing the gene of interest highlighted in purple. Plots produced using Seurat.

4.9 Discussion

This chapter demonstrates a defensive role for IL-22 in the intestinal epithelial response to *S*. Typhimurium infection and outlines a major mechanism by which this is occurring. Restriction of intracellular *M. tuberculosis* growth secondary to IL-22-enhanced phagolysosomal fusion has been demonstrated previously in macrophages[18], but this is the first demonstration of this process with a Gram-negative pathogen, and we show that calgranulin B (S100A9) is required for this process, rather than solely calgranulin A as previously thought.[24] Both calgranulin A and B consist of 2 helix-loop-helix EF binding motifs, which are connected by a hinge region. They can exist as heterodimers or homodimers. After binding with Ca^{2+}, the molecule opens up, exposing a hydrophobic cleft in the hinge region, which binds with the molecule's target protein of interest.[29] It is proposed that IL-22 enhances phagolysosomal fusion by increasing intracellular levels of Ca^{2+}, causing movement of calgranulin A (or in this case, B) to the phagosomal membrane. Following conformational change of the molecule on binding with Ca^{2+}, calgranulin A / B is able to bind with a currently unidentified molecule to increase Rab7 expression and increase phagosomal maturation / bacterial killing.[24] In humans, S100A8 and S100A9 are known to be associated with both immune-related inflammatory disorders such as psoriasis and in infection-related inflammation.[30] Murine studies have demonstrated decreased

phagocytosis of *Klebsiella pneumoniae* by S100A9$^{-/-}$ murine macrophages with increased dissemination of infection,[31] and impaired leukocyte migration in S100A9$^{-/-}$ mice, as well as an important role for S100A8/9 in regulation of cytoskeletal modulation (essential for successful phagocytosis).[32] There is little data on the role of S100A9 in either the murine or human intestinal epithelium; further study would be required to establish the relevance of this pathway for phagolysosomal fusion and bacterial defence in the intact immune system *in vivo*, and to determine what the specific interactions are between S100A9, RAB7 and the phagolysosome.

Data on the IL-22 response in the intact intestinal immune system would be of particular interest, given that in contrast to our findings that IECs appear to be less susceptible to *S*. Typhimurium invasion with a functional IL-22 pathway, IL-22$^{-/-}$ mice were not demonstrated to have any significant difference in susceptibility to *S*. Typhimurium infection.[15] In this case, it may be that antimicrobial peptides whose secretion is induced by IL-22 favoured the growth of non-protective elements of the microbiota, allowing increased colonisation and thus infection with *S*. Typhimurium in wild type mice, whereas although the immune response in IL-22$^{-/-}$ mice may be diminished, their microbiota were less favourable for *S*. Typhimurium colonisation. Additionally it is possible that *Salmonella* were using different methods of crossing the epithelial barrier, such as direct capture from the lumen by phagocytes/dendritic cells, or transfer via M cells; pathways which are not possible in the iHO model.[33]

Our data demonstrate differences in IEC susceptibility to infection after pre-incubation with IL-22, suggesting that this response may be more relevant to later stages of infection, rather than the very early stages whilst the IL-22 pathway is activated. However, constitutive epithelial expression of factors such as IL-17A have been demonstrated in some models to provide initial protection and delay invasion of *S*. Typhimurium,[34] and both IL-22 and IL-22-regulated genes have been demonstrated to be upregulated at early timepoints post-infection,[35,36] suggesting that there could be a role for the defensive mechanism of IL-22 we have outlined in the initial stages of infection.

With regards to the attempt to identify populations of cell subsets and better understand the transcriptional response of each cell type to IL-22, it is clear that despite providing a very

high depth of sequencing, the SmartSeq2 method is too time-consuming and allows limited batches of cells to be processed on a particular occasion. The pipeline is long (2 days to process a plate), and difficulties with cell sorting or either clean up step can lead to plates not being processable at the barcoding stage. In addition, barcoding incurs a large expense per cell, which limited the ability to do this on a large scale during this project. Since the sequencing for this project was done, new methods have come to the fore for this type of work, such as microfluidic techniques, including droplet-based single cell RNA-Seq,[37] which can provide large amounts of data very rapidly. A relevant example would be its use to profile cell populations in the mouse intestine, profiling over 50,000 cells during one experiment.[38] This method allowed not only identification of rare populations such as enteroendocrine cells (thought to represent around 1% of cells in iHO), but their division into specific subpopulations and was also able to demonstrate changes in cell population in response to infection.

The clustering and data analysis techniques used here would similarly work better on larger scale data; as gene filtering in the SC3 programme removes both very rare and ubiquitous transcripts, as analysis has previously demonstrated that these factors do not affect clustering.[26] However, this would make the method less sensitive to picking up rare cell types. It is possible to alter these parameters to provide increased sensitivity but the fact that clustering done with Seurat, which filters only for high mitochondrial reads and specifically searches for genes which display high cell-cell variability (as would have been expected between IL-22 stimulated and unstimulated cells) provided the same types of cell clusters suggests that both were valid tools, but the limitation lay in the number of cells sequenced.

Using a microfluidic-based approach to perform larger-scale single cell sequencing would be an ideal next step to definitively identify cell populations in an *in vitro* human intestinal epithelial model such as the iHO, and study cellular responses to IL-22 treatment and *S*. Typhimurium infection.

References:

1. Schreiber F, Arasteh JM, Lawley TD. Pathogen Resistance Mediated by IL-22 Signaling at the Epithelial-Microbiota Interface. *J Mol Biol.* 2015;427(23):3676-3682.
2. Sabat R, Ouyang W, Wolk K. Therapeutic opportunities of the IL-22-IL-22R1 system. *Nat Rev Drug Discov.* 2014;13(1):21-38.
3. Kotenko SV, Izotova LS, Mirochnitchenko OV, et al. Identification of the functional interleukin-22 (IL-22) receptor complex: the IL-10R2 chain (IL-10Rbeta) is a common chain of both the IL-10 and IL-22 (IL-10-related T cell-derived inducible factor, IL-TIF) receptor complexes. *J Biol Chem.* 2001;276(4):2725-2732.
4. Ranjbar S, Haridas V, Jasenosky LD, Falvo JV, Goldfeld AE. A Role for IFITM Proteins in Restriction of Mycobacterium tuberculosis Infection. *Cell Rep.* 2015;13(5):874-883.
5. Grasberger H, El-Zaatari M, Dang DT, Merchant JL. Dual oxidases control release of hydrogen peroxide by the gastric epithelium to prevent Helicobacter felis infection and inflammation in mice. *Gastroenterology.* 2013;145(5):1045-1054.
6. Flores MV, Crawford KC, Pullin LM, Hall CJ, Crosier KE, Crosier PS. Dual oxidase in the intestinal epithelium of zebrafish larvae has anti-bacterial properties. *Biochem Biophys Res Commun.* 2010;400(1):164-168.
7. Forbester JL, Lees EA, Goulding D, et al. Interleukin-22 promotes phagolysosomal fusion to induce protection against Salmonella enterica Typhimurium in human epithelial cells. *Proc Natl Acad Sci U S A.* 2018;115(40):10118-10123.
8. Sabat R. IL-10 family of cytokines. *Cytokine Growth Factor Rev.* 2010;21(5):315-324.
9. Commins S, Steinke JW, Borish L. The extended IL-10 superfamily: IL-10, IL-19, IL-20, IL-22, IL-24, IL-26, IL-28, and IL-29. *J Allergy Clin Immunol.* 2008;121(5):1108-1111.
10. Glocker EO, Kotlarz D, Boztug K, et al. Inflammatory bowel disease and mutations affecting the interleukin-10 receptor. *N Engl J Med.* 2009;361(21):2033-2045.
11. Spencer SD, Di Marco F, Hooley J, et al. The orphan receptor CRF2-4 is an essential subunit of the interleukin 10 receptor. *J Exp Med.* 1998;187(4):571-578.
12. Pham TA, Clare S, Goulding D, et al. Epithelial IL-22RA1-mediated fucosylation promotes intestinal colonization resistance to an opportunistic pathogen. *Cell Host Microbe.* 2014;16(4):504-516.

13. Zheng Y, Valdez PA, Danilenko DM, et al. Interleukin-22 mediates early host defense against attaching and effacing bacterial pathogens. *Nat Med.* 2008;14(3):282-289.
14. Engelhardt KR, Shah N, Faizura-Yeop I, et al. Clinical outcome in IL-10- and IL-10 receptor-deficient patients with or without hematopoietic stem cell transplantation. *J Allergy Clin Immunol.* 2013;131(3):825-830.
15. Behnsen J, Jellbauer S, Wong CP, et al. The cytokine IL-22 promotes pathogen colonization by suppressing related commensal bacteria. *Immunity.* 2014;40(2):262-273.
16. Muller AJ, Kaiser P, Dittmar KE, et al. Salmonella gut invasion involves TTSS-2-dependent epithelial traversal, basolateral exit, and uptake by epithelium-sampling lamina propria phagocytes. *Cell Host Microbe.* 2012;11(1):19-32.
17. Friedrich N, Hagedorn M, Soldati-Favre D, Soldati T. Prison break: pathogens' strategies to egress from host cells. *Microbiol Mol Biol Rev.* 2012;76(4):707-720.
18. Dhiman R, Indramohan M, Barnes PF, et al. IL-22 produced by human NK cells inhibits growth of Mycobacterium tuberculosis by enhancing phagolysosomal fusion. *J Immunol.* 2009;183(10):6639-6645.
19. Vergne I, Chua J, Deretic V. Tuberculosis toxin blocking phagosome maturation inhibits a novel Ca2+/calmodulin-PI3K hVPS34 cascade. *J Exp Med.* 2003;198(4):653-659.
20. Drose S, Altendorf K. Bafilomycins and concanamycins as inhibitors of V-ATPases and P-ATPases. *J Exp Biol.* 1997;200(Pt 1):1-8.
21. Yates RM, Hermetter A, Russell DG. The kinetics of phagosome maturation as a function of phagosome/lysosome fusion and acquisition of hydrolytic activity. *Traffic.* 2005;6(5):413-420.
22. Mottola G. The complexity of Rab5 to Rab7 transition guarantees specificity of pathogen subversion mechanisms. *Front Cell Infect Microbiol.* 2014;4:180.
23. Via LE, Deretic D, Ulmer RJ, Hibler NS, Huber LA, Deretic V. Arrest of mycobacterial phagosome maturation is caused by a block in vesicle fusion between stages controlled by rab5 and rab7. *J Biol Chem.* 1997;272(20):13326-13331.
24. Dhiman R, Venkatasubramanian S, Paidipally P, Barnes PF, Tvinnereim A, Vankayalapati R. Interleukin 22 inhibits intracellular growth of Mycobacterium

tuberculosis by enhancing calgranulin A expression. *J Infect Dis.* 2014;209(4):578-587.

25. Carrion M, Juarranz Y, Martinez C, et al. IL-22/IL-22R1 axis and S100A8/A9 alarmins in human osteoarthritic and rheumatoid arthritis synovial fibroblasts. *Rheumatology (Oxford).* 2013;52(12):2177-2186.
26. Kiselev VY, Kirschner K, Schaub MT, et al. SC3: consensus clustering of single-cell RNA-seq data. *Nat Methods.* 2017;14(5):483-486.
27. Butler A, Hoffman P, Smibert P, Papalexi E, Satija R. Integrating single-cell transcriptomic data across different conditions, technologies, and species. *Nat Biotechnol.* 2018;36(5):411-420.
28. Hernandez P, Gronke K, Diefenbach A. A catch-22: Interleukin-22 and cancer. *Eur J Immunol.* 2018;48(1):15-31.
29. Marenholz I, Heizmann CW, Fritz G. S100 proteins in mouse and man: from evolution to function and pathology (including an update of the nomenclature). *Biochem Biophys Res Commun.* 2004;322(4):1111-1122.
30. Wang S, Song R, Wang Z, Jing Z, Wang S, Ma J. S100A8/A9 in Inflammation. *Front Immunol.* 2018;9:1298.
31. Achouiti A, Vogl T, Urban CF, et al. Myeloid-related protein-14 contributes to protective immunity in gram-negative pneumonia derived sepsis. *PLoS Pathog.* 2012;8(10):e1002987.
32. Vogl T, Ludwig S, Goebeler M, et al. MRP8 and MRP14 control microtubule reorganization during transendothelial migration of phagocytes. *Blood.* 2004;104(13):4260-4268.
33. Velge P, Wiedemann A, Rosselin M, et al. Multiplicity of Salmonella entry mechanisms, a new paradigm for Salmonella pathogenesis. *Microbiologyopen.* 2012;1(3):243-258.
34. Mayuzumi H, Inagaki-Ohara K, Uyttenhove C, Okamoto Y, Matsuzaki G. Interleukin-17A is required to suppress invasion of Salmonella enterica serovar Typhimurium to enteric mucosa. *Immunology.* 2010;131(3):377-385.
35. Aujla SJ, Chan YR, Zheng M, et al. IL-22 mediates mucosal host defense against Gram-negative bacterial pneumonia. *Nat Med.* 2008;14(3):275-281.

36. Raffatellu M, Santos RL, Verhoeven DE, et al. Simian immunodeficiency virus-induced mucosal interleukin-17 deficiency promotes Salmonella dissemination from the gut. *Nat Med.* 2008;14(4):421-428.
37. Macosko EZ, Basu A, Satija R, et al. Highly Parallel Genome-wide Expression Profiling of Individual Cells Using Nanoliter Droplets. *Cell.* 2015;161(5):1202-1214.
38. Haber AL, Biton M, Rogel N, et al. A single-cell survey of the small intestinal epithelium. *Nature.* 2017;551(7680):333-339.